Draft version July 29, 2021
Typeset using LATEX twocolumn style in AASTeX63

New searches for continuous gravitational waves from seven fast pulsars

A. Ashok,[1,2] B. Beheshtipour,[1,2] M. A. Papa,[1,3,2] P. C. C. Freire,[4] B. Steltner,[1,2] B. Machenschalk,[1,2] O. Behnke,[1,2] B. Allen,[1,3,2] and R. Prix[1,2]

[1] *Max Planck Institute for Gravitational Physics (Albert Einstein Institute), Callinstrasse 38, 30167 Hannover, Germany*
[2] *Leibniz Universität Hannover, D-30167 Hannover, Germany*
[3] *University of Wisconsin Milwaukee, 3135 N Maryland Ave, Milwaukee, WI 53211, USA*
[4] *Max-Planck-Institut für Radioastronomie, Auf dem Hügel 69, D-53121 Bonn, Germany*

ABSTRACT

We conduct searches for continuous gravitational waves from seven pulsars, that have not been targeted in continuous wave searches of Advanced LIGO data before. We target emission at exactly twice the rotation frequency of the pulsars and in a small band around such frequency. The former search assumes that the gravitational wave quadrupole is changing phase-locked with the rotation of the pulsar. The search over a range of frequencies allows for differential rotation between the component emitting the radio signal and the component emitting the gravitational waves, for example the crust or magnetosphere versus the core. Timing solutions derived from the Arecibo 327-MHz Drift-Scan Pulsar Survey (AO327) observations are used. No evidence of a signal is found and upper limits are set on the gravitational wave amplitude. For one of the pulsars we probe gravitational wave intrinsic amplitudes just a factor of 3.8 higher than the spin-down limit, assuming a canonical moment of inertia of 10^{38} kg m^2. Our tightest ellipticity constraint is 1.5×10^{-8}, which is a value well within the range of what a neutron star crust could support.

Keywords: continuous gravitational waves, neutron stars

1. INTRODUCTION

Continuous gravitational waves are expected from rotating neutron stars if these objects present a deviation from a perfectly axisymmetric configuration (Lasky 2015; Jaranowski et al. 1998). On the whole, the expected signal is simple, consisting of one or two harmonics, at the rotation frequency of the star and at twice this frequency (Jones 2015).

The sensitivity of the LIGO instruments allows to probe continuous gravitational wave emission from the Galactic population of neutron stars, for deformations of a few parts in a million and smaller, depending on the search, over a broad range of frequencies. Different types of searches are carried out: "blind" all-sky surveys (Abbott et al. 2021a; Steltner et al. 2021b; Covas & Sintes 2020; Dergachev & Papa 2021, 2020; Abbott et al. 2019a), searches directed at neutron star candidates like supernova remnants, low mass X-ray binaries (Zhang et al. 2021; Abbott et al. 2021b; Papa et al. 2020; Lindblom & Owen 2020; Jones & Sun 2021; Ming et al. 2019) and targeted searches aimed at known pulsars (Abbott et al. 2019b,c; Nieder et al. 2020, 2019; Fesik & Papa 2020; Abbott et al. 2021c,d).

Among the different searches, the ones that target pulsars, have a special place. Pulsars are believed to be neutron stars, the distance is usually known and the rotation frequency and its derivatives are also known. This has important consequences: a null measurement is directly informative on the gravitational wave emission – there is no question about whether a source is there in the first place. The search is simple because whatever the emission mechanism is, the gravitational frequency depends on the spin frequency, which is known. A detection would therefore immediately encode information on what is sourcing the gravitational waves. Because there is little to no uncertainty on the gravitational waveform from a known pulsar, the number of templates that are

Corresponding author: A. Ashok
anjana.ashok@aei.mpg.de

Corresponding author: M.A. Papa
maria.alessandra.papa@aei.mpg.de

searched is many orders of magnitude smaller than those investigated in surveys, and this makes these searches the most sensitive: the smallest detectable signal is a few times smaller than what the most sensitive broad survey could detect at the same frequency.

In this paper we present results from searches for emission from seven new pulsars using public data from all three Advanced LIGO observing runs O1, O2 and O3 (Abbott et al. 2021e; LIGO 2019a,b,c).

The plan of the paper is the following: we introduce the signal model in Section 2. In Sections 3 we detail the targeted objects. The gravitational wave searches are described in 4, the results are presented and discussed in 5.

2. THE SIGNAL

The search described in this paper targets nearly monochromatic gravitational wave signals of the form described for example in Section II of Jaranowski et al. (1998). In the calibrated strain data from a gravitational wave detector the signal has the form

$$h(t) = F_+(\alpha,\delta,\psi;t)h_+(t) + F_\times(\alpha,\delta,\psi;t)h_\times(t), \quad (1)$$

with the "+" and "×" indicating the two gravitational wave polarizations. $F_+(\alpha,\delta,\psi;t)$ and $F_\times(\alpha,\delta,\psi;t)$ are the detector sensitivity pattern functions, which depend on relative orientation between the detector and the source, and hence on time t, on the position (α,δ) of the source, and on ψ, the polarization angle. The waveforms $h_+(t)$ and $h_\times(t)$ are

$$\begin{aligned} h_+(t) &= A_+ \cos\Phi(t) \\ h_\times(t) &= A_\times \sin\Phi(t), \end{aligned} \quad (2)$$

with

$$\begin{aligned} A_+ &= \frac{1}{2}h_0(1+\cos^2\iota) \\ A_\times &= h_0\cos\iota. \end{aligned} \quad (3)$$

The angle between the total angular momentum of the star and the line of sight is $0 \le \iota \le \pi$ and $h_0 \ge 0$ is the intrinsic gravitational wave amplitude. $\Phi(t)$ of Eq. 2 is the phase of the gravitational wave signal at time t. If τ_{SSB} is the arrival time of the wave with phase $\Phi(t)$ at the solar system barycenter, then $\Phi(t) = \Phi(\tau_{\mathrm{SSB}}(t))$. The gravitational wave phase as function of τ_{SSB} is assumed to be

$$\Phi(\tau_{\mathrm{SSB}}) = \Phi_0 + 2\pi[f(\tau_{\mathrm{SSB}} - \tau_{0\mathrm{SSB}}) + \frac{1}{2}\dot{f}(\tau_{\mathrm{SSB}} - \tau_{0\mathrm{SSB}})^2]. \quad (4)$$

We take $\tau_{0\mathrm{SSB}}$ consistently with the timing solution, and hence different for every pulsar, as shown in Table 3.

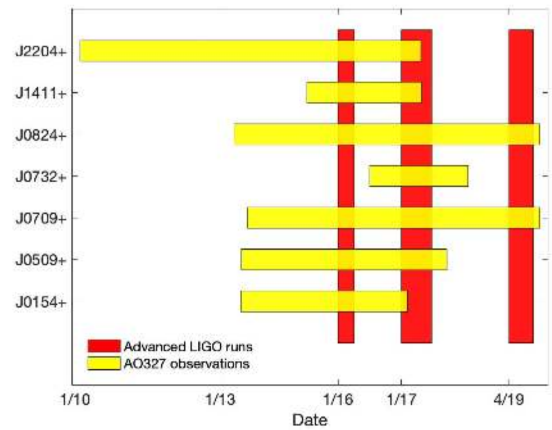

Figure 1. Time intervals corresponding to the O1, O2, and O3 LIGO runs are shown in red as "vertical rectangles" and the radio observation periods for each pulsar are shown in yellow as "horizontal rectangles".

3. THE PULSARS

We target continuous gravitational wave emission from seven recycled pulsars discovered and/or timed with data from the Arecibo 327-MHz Drift-Scan Pulsar Survey (AO327) (Martinez et al. 2019, 2017): PSR J2204+2700, PSR J1411+2551, PSR J0709+0458, PSR J0824+0028, PSR J0732+2314, PSR J0509+0856 and PSR J0154+1833. For practicality we mostly use abbreviated forms of the names of the pulsars, omitting the "PSR" prefix and the part after the "+".

These pulsars have never been searched before, for gravitational wave emission. They represent a relatively nearby sample, with distances smaller than 2 kpc, which is typical of all-sky surveys. This makes them particularly interesting for gravitational wave searches, the only exception being 2204+2700, which is more distant, and also having an extremely low spindown.

Our targets are all in binary systems except for J0154+1833, that is an isolated millisecond pulsar. Our set includes the radio pulsar in the notable double-neutron star system PSR J1411+2551.

When available, we take the orbital inclination angle as estimate of the inclination angle ι for the determination of the constrained prior upper limit, see Section 5.1. We take the following values: $\iota_{J1411} = 0.83$ rad, $\iota_{J0709} = 1.30$ rad, $\iota_{J0824} = 1.32$ rad, $\iota_{0732} = 0.93$ rad. For J0154, J0509 and J2204 we do not have an estimate of the inclination angle.

4. THE GRAVITATIONAL WAVE SEARCHES

We use LIGO public data from the Hanford (H1) and the Livingston (L1) detectors from the O1, O2 and the recently released first six months of the O3 science run (LIGO 2019a,b,c). The data is gated to remove loud glitches (Steltner et al. 2021a) and contiguous segments are Fourier-transformed to produce the input to the search. After having excluded egregiously noisy segments in the band of each pulsar, we have ≈ 175 days of data from each detector from the O1 and O2 runs combined, and ≈ 125 during the O3 run for H1 and ≈ 129 days for L1.

No glitch was recorded by the AO327 in any of the pulsars' spins. As Figure 1 shows, these observations do not perfectly cover all the Advanced LIGO runs so we cannot exclude the possibility of a glitch. Even though our targets are very stable pulsars and a glitch is unlikely, we perform different searches and combine coherently the O1 and O2 data, the O3 data, and also all the data that we have, O1O2O3. We use the matched-filter detection statistic – $\mathcal{F}$-statistic (Cutler & Schutz 2005) – as our detection statistic. The $\mathcal{F}$-statistic is the maximum log-likelihood ratio of the signal hypothesis to the Gaussian noise hypothesis. The signal is described by a frequency, spindown, sky-position and orbital parameter values, which define the template waveform and are explicitly searched over. The signal amplitude parameters $\cos\iota$, ψ, Φ_0 and h_0 are analytically maximised over.

In Gaussian noise the $2\mathcal{F}$-statistic follows a non-central chi-squared distribution with 4 degrees of freedom, ${\chi^2}_4(\rho^2)$. The non-centrality parameter ρ^2 is the expected squared signal-to-noise ratio and it is proportional to $h_0^2 T_{\rm data}/S_h$, where $T_{\rm data}$ is the duration of time for which data is available and S_h is the strain power spectral density of the noise (Jaranowski et al. 1998).

For every pulsar and data set we conduct two searches: one with a single template with the gravitational wave frequency f and spindown $\dot{f}$ being twice the spin frequency ν and spindown $\dot{\nu}$, and one for a range of frequencies and spindowns around these. The parameters of the targeted searches are given in Table 3 in the appendix.

The search at $f = 2\nu$ is appropriate if the gravitational wave frequency is exactly locked with the observed spin frequency. Mechanisms however exist that could produce a small difference between the gravitational wave frequency and twice the spin frequency: a misalignment of the rotation axis with the symmetry axis of the star, causing free precession; or the component responsible for the gravitational wave emission – for example a solid core – not spinning as the radio-emitting component. In such cases $f = 2\nu(1 \pm \delta_f)$ with $\delta_f \lesssim 10^{-4}$ (Jones & Andersson 2002; Abbott et al. 2008). With this in mind, we conservatively perform searches over a band $\pm 2\nu \times 2 \cdot 10^{-3}$ of $f = 2\nu$, and consistently for $\dot{f}$.

For the band searches we set up a template grid in frequency and spin-down with spacings of 2.6×10^{-9} Hz and 1.9×10^{-17} Hz/s, respectively. These grids yield a maximum mismatch smaller than 1% for the O1O2 and O3 searches, and smaller than 8% for the O1O2O3 searches.

We also conduct the single-template searches using a Bayesian search. This method demodulates the data according to the expected signal, heterodynes/downsamples the data and then searches over the waveform amplitude parameters with a nested sampling algorithm, see for example (Abbott et al. 2019d). The data used for this search is not gated. We report the results for the combined O1O2O3 data.

5. RESULTS

None of the targeted searches yield a detection. Figure 2 shows the Gaussian noise p-values for the targeted searches (blue circles): All the results for the targeted searches are consistent with the noise-only hypothesis. The most significant targeted-search result comes from PSR J0709 from the O3-data search, with a p-value is $\approx$ 23%. PSR J0709 yields the lowest combined O1O2+O3 p-value at a level of $\approx$ 12%. However the coherent O1O2O3 data search yields a totally insignificant p-value of $\approx$ 83% . The Bayesian posteriors of Figure 3 are consistent with the $\mathcal{F}$-stat results, with the only slightly off-zero posterior found for PSR J0709. Such posterior is very broad, includes zero and may happen just due to Gaussian fluctuations. We also note that the target frequency for PSR J0709 is at $\approx$ 58 Hz which is a highly contaminated region.

To evaluate the results from the band-searches, for every pulsar we consider the most significant result in each 10 mHz band and compute the Gaussian-noise p-value associated with it. These are the red circles shown in the left-hand-side plots in the first three rows of Figure 2. The larger is the band that has been searched, the lower is the lowest p-value recorded for that pulsar, so in order to directly compare the significance of results from different pulsars we multiply each p-value by the number of 10 mHz bands searched for each pulsar. These new rescaled p-values are shown in the right-hand-side plots of Figure 2. The most significant results from the band searches comes again from PSR J0709, in the O1O2O3 coherent search and is at the level of $\approx$ 9%. However this significance is not confirmed in the O1O2+O3 data where the rescaled most significant result has a p-value higher than 80%. The remaining p-values are all larger than 15%.

Figures 4 show the distributions of the most significant 10 mHz p-values and illustrate that they are consistent

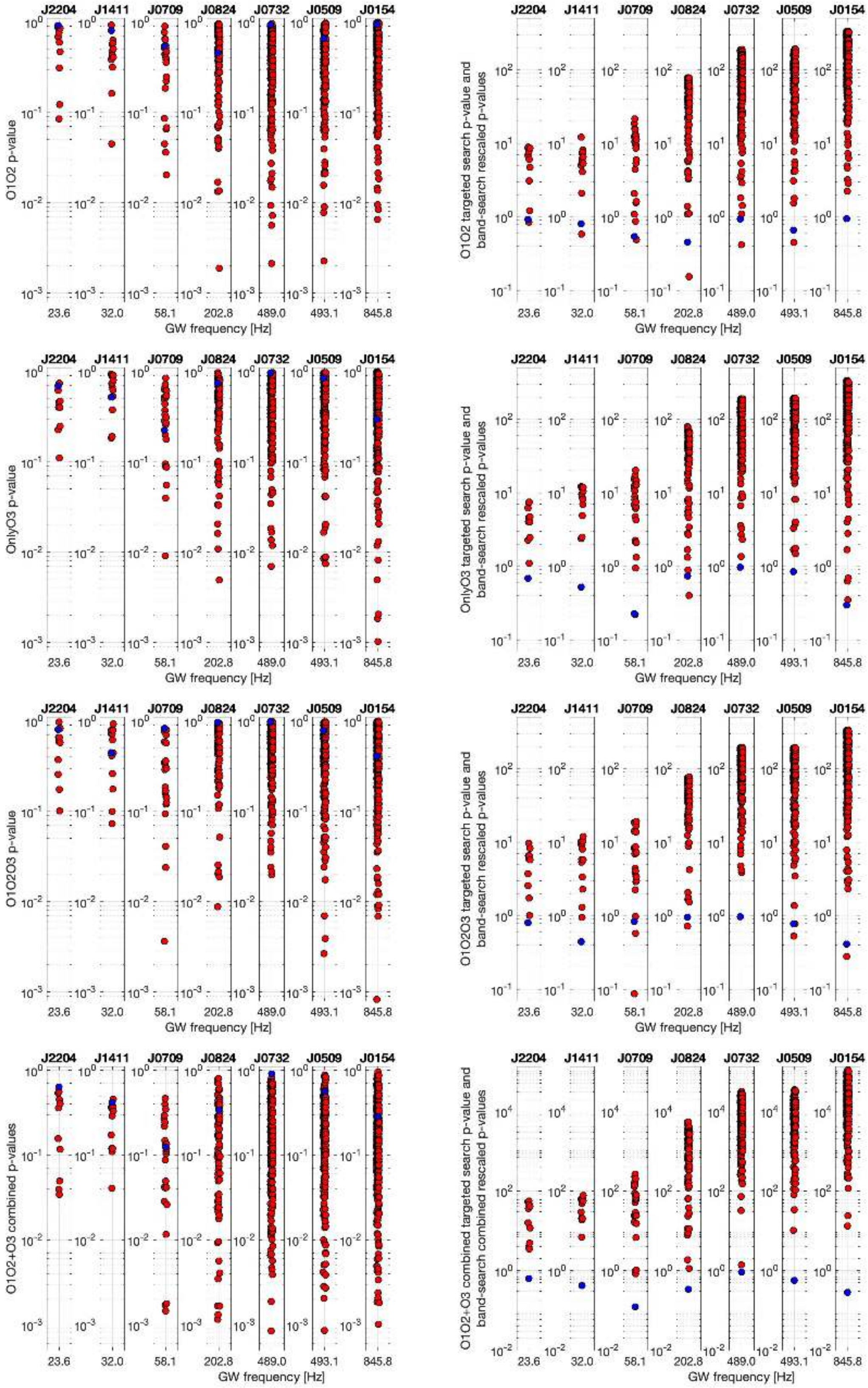

Figure 2. O1O2 (1st row), O3 (2nd row) , O1O2O3 (3rd row) and O1O2+O3 (4th row) results. For each 10 mHz frequency band searched, we show the Gaussian p-value of the most significant result at the waveform frequency (red circles). The darker (blue) circles show the p-values of the targeted searches. These are generally lower than the bulk of the values from the band-search because the latter are maxima over 10 mHz, whereas the targeted searches probe only a single waveform. The red circles in the right hand-side plot are the red circles in the left-side plot each multiplied by the number of 10 mHz bands searched for that pulsar. For low p-values these can be taken as a measure of the significance and may be used to compare results for different pulsars. The 4th row shows the combinations of the O1O2 and O3 results, obtained by multiplying the p-values from these searches.

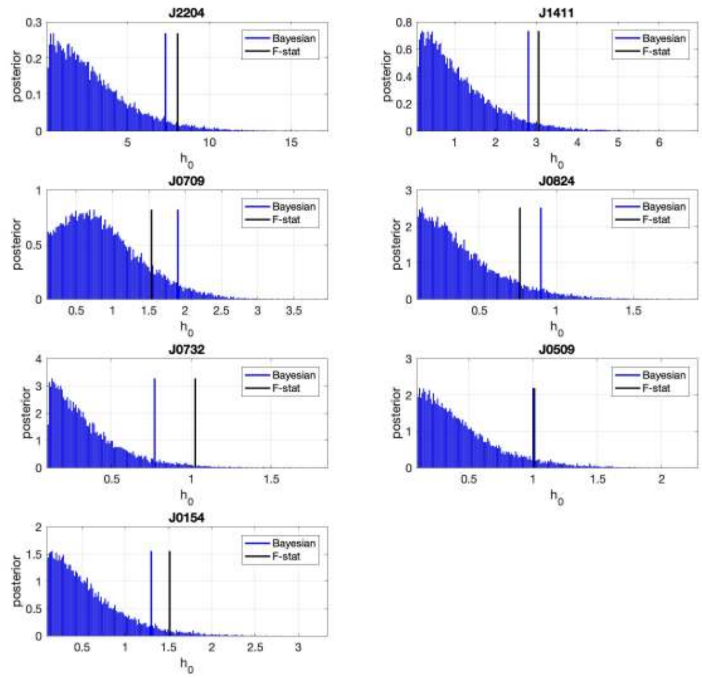

Figure 3. Bayesian posteriors for the combined O1O2O3 searches (blue) and associated 95% confidence upper limits. We also show (black) the $\mathcal{F}$-stat upper limits.

with the Gaussian-noise expectations for searches on all data.

5.1. *Upper limits*

Based on the O1O2, O3 and O1O2O3 targeted search results we place 95% confidence upper limits on the intrinsic gravitational wave amplitude at the detector h_0 defined in Eq. 3. We use a series of Monte Carlos where we simulate signals at fixed amplitude in real data and measure the detection efficiency of our search. The detection criteria is that the obtained value of the detection statistic be equal or greater than the one found in the real search: if the measured detection statistic is high, a higher gravitational wave amplitude will be needed in order for the signals to be detected. The amplitude for which 95% of the tested signals is detected, is the upper limit value, $h_0^{95\%}$. With minor variations on the theme, this is the standard approach that we have taken for $\mathcal{F}$-statistic searches since the very first continuous waves search on LIGO data back in 2004. The $\mathcal{F}$-stat upper limits are shown in Tables 1. The Bayesian upper limits are readily derived from the posteriors of Fig. 3 and are shown in Table 2.

For the O1O2 band-searches we divide the searched frequency range in 10 mHz sub-bands and take the most significant detection statistic value in that sub-band for our detection criteria. The sub-band searches probe numerous waveforms and so the loudest detection statistic

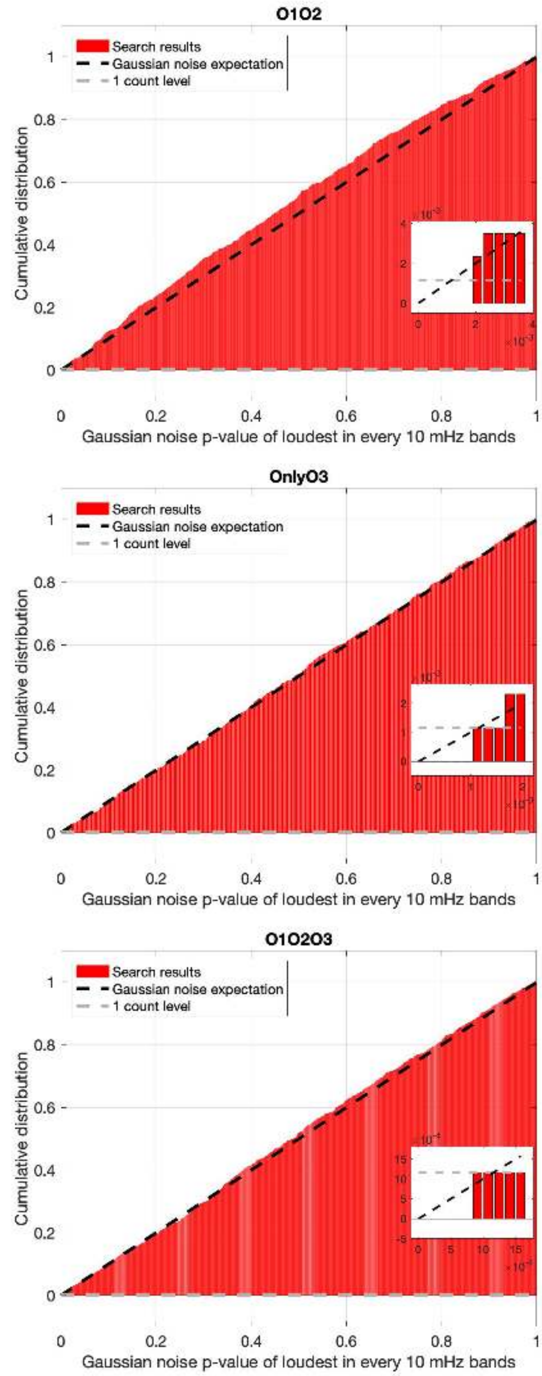

Figure 4. O1O2, O3 and O1O2O3 band-search results. For each 10 mHz frequency band searched, we show the cumulative distribution of the Gaussian p-value of the most significant result. If the data were Gaussian noise, the distribution would follow the dashed black line.

value is going to be higher than for the targeted searches. Correspondingly the upper limits will also be higher as shown in Figure 5 in the appendix, typically by a factor of ≈ 2.7. Since this is the most computationally intense part of this work, and we do not find evidence for a signal, we do not set upper limits based on the O3 data, or on the O1O2O3, but we expect that these would be higher than the corresponding targeted ones by also a factor of a few.

The populations of fake signals used to determine the detection efficiencies have polarization angle ψ uniformly distributed with $|\psi| \leq \pi/4$ and initial phase Φ_0 uniformly distributed in $[0, 2\pi)$. For the orientation angle we consider two cases: $\cos\iota$ uniformly distributed in $[-1, 1)$ and fixed at the value of the orbital inclination, when available from the radio observations. We refer to the resulting upper limits as *unconstrained* and *constrained*, respectively.

If we assume that the neutron star is a triaxial ellipsoid spinning around a principal moment of inertia axis I_{zz}, and that the continuous wave emission is due to an ellipticity

$$\varepsilon = \frac{I_{xx} - I_{yy}}{I_{zz}}, \tag{5}$$

based on the intrinsic gravitational wave amplitude upper limits $h_0^{95\%}$, we can exclude neutron star deformations above a $\varepsilon^{95\%}$ level. The ellipticity needed for a neutron star at a distance D, spinning at $f/2$, to produce continuous gravitational waves with an intrinsic amplitude on Earth of h_0 is (Jaranowski et al. 1998; Gao et al. 2020):

$$\varepsilon = 2.4 \times 10^{-7} \left(\frac{h_0}{1 \times 10^{-26}}\right) \times \left(\frac{D}{1\ \mathrm{kpc}}\right)\left(\frac{200\ \mathrm{Hz}}{f}\right)^2 \left(\frac{10^{38}\ \mathrm{kg\ m}^2}{I_{zz}}\right). \tag{6}$$

The ellipticity $\varepsilon^{95\%}$ upper limits are given in Table 1.

5.2. *Discussion*

We have searched for continuous gravitational waves from seven pulsars that have not been targeted before. We use all the publicly available Advanced LIGO data, namely from the O1, O2 and O3 science runs.

We find no evidence of a gravitational wave signal at a detectable level. The posterior probability distribution for PSR J0709 is peaked slightly off-zero, but this could well be a Gaussian noise fluctuation as well as due to spectral contamination. Especially at the lower frequencies it is not uncommon to find these posteriors, see for example Figure 3 of (Abbott et al. 2020) showing the results for the Vela Pulsar from the search at ≈ 22 Hz.

For more than half of the pulsar sample, our searches probe ellipticities $\lesssim 3 \times 10^{-7}$, which could be sustained by neutron star crusts (Johnson-McDaniel & Owen 2013; Gittins et al. 2020; Bhattacharyya 2020). Our tightest ellipticity bound amounts to 1.7×10^{-8}, for PSR J0154. The remaining four pulsars are more distant and/or spin slower, which yields less constraining ellipticity upper limits. For the pulsar PSR J0824, assuming a canonical moment of inertia of 10^{38}kg m^2, our upper limits are within a factor of 3.8 (5.8) of the spindown upper limit, for an unconstrained and constrained $\cos\iota$ prior respectively. The actual moment of inertia of the star may differ from the canonical one up by a factor of a few. These are physically interesting ellipticity ranges (Woan et al. 2018), and showcase the potential for this type of search.

ACKNOWLEDGMENTS

All the computational work for these searches was performed on the ATLAS cluster at AEI Hannover. We thank Carsten Aulbert and Henning Fehrmann for their support.

We would like to especially thank the instrument-scientist and engineers of LIGO whose amazing work has produced detectors capable of probing gravitational waves so incredibly small.

This research has made use of data, software and/or web tools obtained from the Gravitational Wave Open Science Center (https://www.gw-openscience.org/), a service of LIGO Laboratory, the LIGO Scientific Collaboration and the Virgo Collaboration. LIGO Laboratory and Advanced LIGO are funded by the United States National Science Foundation (NSF) as well as the Science and Technology Facilities Council (STFC) of the United Kingdom, the Max-Planck-Society (MPS), and the State of Niedersachsen/Germany for support of the construction of Advanced LIGO and construction and operation of the GEO600 detector. Additional support for Advanced LIGO was provided by the Australian Research Council. Virgo is funded, through the European Gravitational Observatory (EGO), by the French Centre National de Recherche Scientifique (CNRS), the Italian Istituto Nazionale di Fisica Nucleare (INFN) and the Dutch Nikhef, with contributions by institutions from Belgium, Germany, Greece, Hungary, Ireland, Japan, Monaco, Poland, Portugal, Spain.

REFERENCES

Abbott, B., et al. 2004, Phys. Rev. D, 69, 082004, doi: 10.1103/PhysRevD.69.082004

—. 2008, Astrophys. J. Lett., 683, L45, doi: 10.1086/591526

Table 1. 95% confidence upper limits on the gravitational wave amplitude for the targeted searches based on no assumptions on the inclination angle (unconstrained prior) and if the inclination angle is the same as the estimated value of the orbital inclination angle (constrained prior), using different data. We also show the spindown upper limit calculated for a nominal value of the moment of inertia of 10^{38} kg m^2, and the spindown limit gravitational wave amplitude. The last two columns indicate how far our results are from being physically interesting: if $h_0^{95\%}/h_0^{\rm spdwn}$ is less than one, then the upper limits are informative.

O1 O2 Pulsar	f [Hz]	$h_0^{95\%}$ UNCONSTRAINED PRIOR	$h_0^{95\%}$ CONSTRAINED PRIOR	$h_0^{\rm spdwn}$	$\epsilon^{95\%}$ UNCONSTRAINED PRIOR	$\epsilon^{95\%}$ CONSTRAINED PRIOR	$h_0^{95}/h_0^{\rm spdwn}$ UNCONSTRAINED PRIOR	$h_0^{95}/h_0^{\rm spdwn}$ CONSTRAINED PRIOR
J0154	≈ 845.8	$2.7^{+0.5}_{-0.5} \times 10^{-26}$	-	9.0×10^{-28}	3.1×10^{-8}	-	30.3	-
J0509	≈ 493.1	$1.9^{+0.5}_{-0.4} \times 10^{-26}$	-	5.2×10^{-28}	1.1×10^{-7}	-	36.3	-
J0709	≈ 58.1	$3.3^{+0.5}_{-0.6} \times 10^{-26}$	$3.9^{+0.6}_{-0.7} \times 10^{-26}$	1.5×10^{-27}	1.6×10^{-5}	2.0×10^{-5}	21.9	26.5
J0732	≈ 489.0	$1.9^{+0.5}_{-0.4} \times 10^{-26}$	$1.4^{+0.4}_{-0.4} \times 10^{-26}$	5.8×10^{-28}	1.2×10^{-7}	9.2×10^{-8}	32.0	24.0
J0824	≈ 202.8	$1.4^{+0.3}_{-0.3} \times 10^{-26}$	$1.8^{+0.4}_{-0.4} \times 10^{-26}$	2.0×10^{-27}	4.9×10^{-7}	6.2×10^{-7}	6.9	8.8
J1411	≈ 32.0	$5.2^{+1.2}_{-1.4} \times 10^{-26}$	$3.6^{+0.9}_{-0.9} \times 10^{-26}$	1.1×10^{-27}	4.7×10^{-5}	3.2×10^{-5}	47.7	32.9
J2204	≈ 23.6	$1.5^{+0.4}_{-0.3} \times 10^{-25}$	-	4.8×10^{-28}	5.6×10^{-4}	-	319.2	-

O3 Pulsar	f [Hz]	$h_0^{95\%}$ UNCONSTRAINED PRIOR	$h_0^{95\%}$ CONSTRAINED PRIOR	$h_0^{\rm spdwn}$	$\epsilon^{95\%}$ UNCONSTRAINED PRIOR	$\epsilon^{95\%}$ CONSTRAINED PRIOR	$h_0^{95}/h_0^{\rm spdwn}$ UNCONSTRAINED PRIOR	$h_0^{95}/h_0^{\rm spdwn}$ CONSTRAINED PRIOR
J0154	≈ 845.8	$1.9^{+0.4}_{-0.3} \times 10^{-26}$	-	9.0×10^{-28}	2.2×10^{-8}	-	21.2	-
J0509	≈ 493.1	$1.2^{+0.2}_{-0.3} \times 10^{-26}$	-	5.2×10^{-28}	6.9×10^{-8}	-	23.7	-
J0709	≈ 58.1	$2.2^{+0.3}_{-0.4} \times 10^{-26}$	$2.4^{+0.3}_{-0.1} \times 10^{-26}$	1.5×10^{-27}	1.1×10^{-5}	1.2×10^{-5}	14.6	16.1
J0732	≈ 489.0	$1.2^{+0.3}_{-0.3} \times 10^{-26}$	$10.0^{+2.5}_{-2.5} \times 10^{-27}$	5.8×10^{-28}	7.9×10^{-8}	6.6×10^{-8}	20.6	17.1
J0824	≈ 202.8	$9.9^{+1.5}_{-1.4} \times 10^{-27}$	$1.2^{+0.2}_{-0.3} \times 10^{-26}$	2.0×10^{-27}	3.5×10^{-7}	4.2×10^{-7}	5.0	5.9
J1411	≈ 32.0	$3.9^{+1.1}_{-1.1} \times 10^{-26}$	$2.7^{+0.7}_{-0.7} \times 10^{-26}$	1.1×10^{-27}	3.5×10^{-5}	2.5×10^{-5}	35.7	25.1
J2204	≈ 23.6	$9.9^{+2.6}_{-2.4} \times 10^{-26}$	-	4.8×10^{-28}	3.6×10^{-4}	-	204.0	-

O1 O2 O3 Pulsar	f [Hz]	$h_0^{95\%}$ UNCONSTRAINED PRIOR	$h_0^{95\%}$ CONSTRAINED PRIOR	$h_0^{\rm spdwn}$	$\epsilon^{95\%}$ UNCONSTRAINED PRIOR	$\epsilon^{95\%}$ CONSTRAINED PRIOR	$h_0^{95}/h_0^{\rm spdwn}$ UNCONSTRAINED PRIOR	$h_0^{95}/h_0^{\rm spdwn}$ CONSTRAINED PRIOR
J0154	≈ 845.8	$1.5^{+0.3}_{-0.3} \times 10^{-26}$	-	9.0×10^{-28}	1.7×10^{-8}	-	16.7	-
J0509	≈ 493.1	$1.0^{+0.2}_{-0.3} \times 10^{-26}$	-	5.2×10^{-28}	5.7×10^{-8}	-	19.6	-
J0709	≈ 58.1	$1.5^{+0.3}_{-0.3} \times 10^{-26}$	$1.9^{+0.3}_{-0.4} \times 10^{-26}$	1.5×10^{-27}	7.7×10^{-6}	9.5×10^{-6}	10.3	12.7
J0732	≈ 489.0	$1.0^{+0.3}_{-0.3} \times 10^{-26}$	$7.8^{+2.5}_{-2.0} \times 10^{-27}$	5.8×10^{-28}	6.7×10^{-8}	5.1×10^{-8}	17.6	13.3
J0824	≈ 202.8	$7.6^{+1.6}_{-1.9} \times 10^{-27}$	$1.2^{+0.3}_{-0.2} \times 10^{-26}$	2.0×10^{-27}	2.7×10^{-7}	4.1×10^{-7}	3.8	5.8
J1411	≈ 32.0	$3.1^{+0.7}_{-0.7} \times 10^{-26}$	$2.2^{+0.4}_{-0.3} \times 10^{-26}$	1.1×10^{-27}	2.8×10^{-5}	2.0×10^{-5}	28.0	19.9
J2204	≈ 23.6	$8.1^{+2.0}_{-2.1} \times 10^{-26}$	-	4.8×10^{-28}	2.9×10^{-4}	-	166.4	-

Table 2. O1-O2-O3 targeted searches Bayesian upper limits (unconstrained $\cos\iota$ priors).

O1 O2 O3 Bayesian Pulsar	$h_0^{95\%}$	$\epsilon^{95\%}$	$h_0^{95}/h_0^{\rm spdwn}$	
J0154	1.3×10^{-26}	1.5×10^{-8}	14.9	-
J0509	1.0×10^{-26}	5.9×10^{-8}	20.1	-
J0709	1.9×10^{-26}	9.4×10^{-6}	12.5	
J0732	7.7×10^{-27}	5.1×10^{-8}	13.2	
J0824	9.0×10^{-27}	3.2×10^{-7}	4.5	
J1411	2.8×10^{-26}	2.5×10^{-5}	25.9	
J2204	7.3×10^{-26}	2.7×10^{-4}	151.4	

Abbott, B. P., et al. 2019a, Phys. Rev., D100, 024004, doi: 10.1103/PhysRevD.100.024004

—. 2019b, Astrophys. J., 879, 10, doi: 10.3847/1538-4357/ab20cb

—. 2019c, Phys. Rev. D, 99, 122002, doi: 10.1103/PhysRevD.99.122002

—. 2019d, Astrophys. J., 879, 10, doi: 10.3847/1538-4357/ab20cb

Abbott, R., et al. 2020, Astrophys. J. Lett., 902, L21, doi: 10.3847/2041-8213/abb655

—. 2021a. https://arxiv.org/abs/2107.00600

—. 2021b. https://arxiv.org/abs/2105.11641

—. 2021c, Astrophys. J., 913, L27, doi: 10.3847/2041-8213/abffcd

—. 2021d. https://arxiv.org/abs/2104.14417

—. 2021e, SoftwareX, 13, 012021, doi: https://doi.org/10.1016/j.softx.2021.100658

Bhattacharyya, S. 2020, The permanent ellipticity of the neutron star in PSR J1023+0038, doi: 10.1093/mnras/staa2304

Covas, P. B., & Sintes, A. M. 2020, Phys. Rev. Lett., 124, 191102, doi: 10.1103/PhysRevLett.124.191102

Cutler, C., & Schutz, B. F. 2005, Phys. Rev. D, 72, 063006, doi: 10.1103/PhysRevD.72.063006

Dergachev, V., & Papa, M. A. 2020, Results from the first all-sky search for continuous gravitational waves from small-ellipticity sources, doi: 10.1103/PhysRevLett.125.171101

—. 2021, Phys. Rev. D, 103, 063019, doi: 10.1103/PhysRevD.103.063019

Fesik, L., & Papa, M. A. 2020, Astrophys. J., 895, 11, doi: 10.3847/1538-4357/ab8193

Gao, Y., Shao, L., Xu, R., et al. 2020, Mon. Not. Roy. Astron. Soc., 498, 1826, doi: 10.1093/mnras/staa2476

Gittins, F., Andersson, N., & Jones, D. 2020. https://arxiv.org/abs/2009.12794

Jaranowski, P., Krolak, A., & Schutz, B. F. 1998, Phys. Rev., D58, 063001, doi: 10.1103/PhysRevD.58.063001

Johnson-McDaniel, N. K., & Owen, B. J. 2013, Phys. Rev. D, 88, 044004, doi: 10.1103/PhysRevD.88.044004

Jones, D., & Sun, L. 2021, Phys. Rev. D, 103, 023020, doi: 10.1103/PhysRevD.103.023020

Jones, D. I. 2015, Mon. Not. Roy. Astron. Soc., 453, 53, doi: 10.1093/mnras/stv1584

Jones, D. I., & Andersson, N. 2002, Mon. Not. Roy. Astron. Soc., 331, 203, doi: 10.1046/j.1365-8711.2002.05180.x

Lasky, P. D. 2015, Publ. Astron. Soc. Austral., 32, e034, doi: 10.1017/pasa.2015.35

LIGO. 2019a, The O2 Data Release, https://www.gw-openscience.org/O1/, doi: 10.7935/K57P8W9D

—. 2019b, The O2 Data Release, https://www.gw-openscience.org/O2/, doi: 10.7935/CA75-FM95

—. 2019c, The O2 Data Release, https://www.gw-openscience.org/O2/, doi: 10.7935/nfnt-hm34

Lindblom, L., & Owen, B. J. 2020, Phys. Rev. D, 101, 083023, doi: 10.1103/PhysRevD.101.083023

Martinez, J. G., Stovall, K., Freire, P. C. C., et al. 2017, Astrophys. J. Lett., 851, L29, doi: 10.3847/2041-8213/aa9d87

Martinez, J. G., Gentile, P., Freire, P. C. C., et al. 2019, Astrophys. J., 881, 166, doi: 10.3847/1538-4357/ab2877

Ming, J., Papa, M. A., Singh, A., et al. 2019, Phys. Rev., D100, 024063, doi: 10.1103/PhysRevD.100.024063

Nieder, L., et al. 2019, doi: 10.3847/1538-4357/ab357e

—. 2020, Astrophys. J. Lett., 902, L46, doi: 10.3847/2041-8213/abbc02

Papa, M. A., Ming, J., Gotthelf, E. V., et al. 2020, Astrophys. J., 897, 22, doi: 10.3847/1538-4357/ab92a6

Steltner, B., Papa, M. A., & Eggenstein, H.-B. 2021a. https://arxiv.org/abs/2105.09933

Steltner, B., Papa, M. A., Eggenstein, H. B., et al. 2021b, Astrophys. J., 909, 79, doi: 10.3847/1538-4357/abc7c9

Woan, G., Pitkin, M., Haskell, B., Jones, D., & Lasky, P. 2018, Astrophys. J. Lett., 863, L40, doi: 10.3847/2041-8213/aad86a

Zhang, Y., Papa, M. A., Krishnan, B., & Watts, A. L. 2021, Astrophys. J. Lett., 906, L14, doi: 10.3847/2041-8213/abd256

APPENDIX

A. ADDITIONAL PLOTS

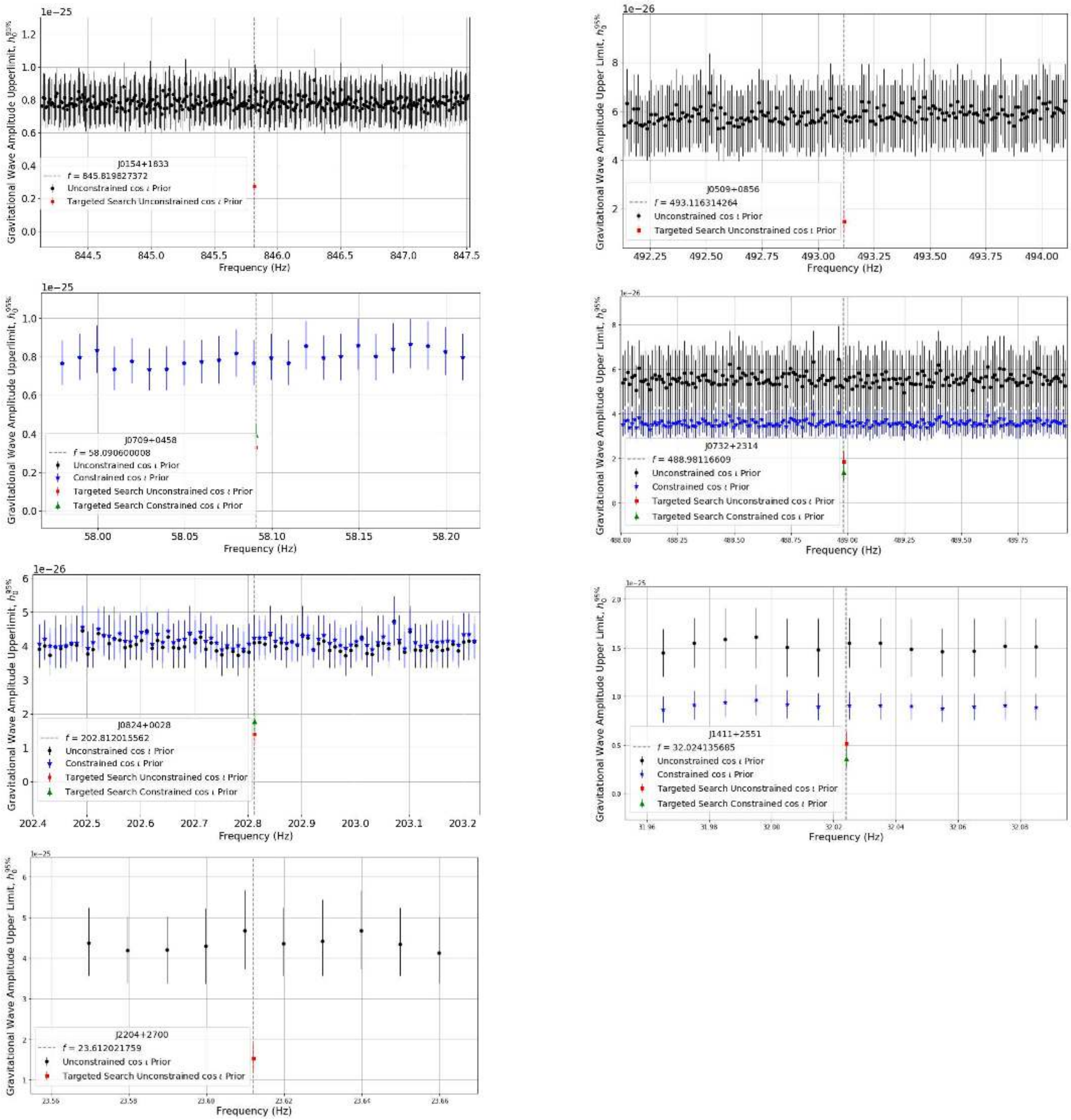

Figure 5. O1O2 data upper limits on the gravitational wave amplitude in each 10 mHz frequency band searched, based on the most significant result in that 10 mHz band. We also show the targeted search results, which are the lower points at the central frequency, which is twice the pulsar rotation frequency.

B. GRAVITATIONAL WAVEFORM PARAMETERS

Table 3. Gravitational waveform parameters

PULSAR	GW frequency f [Hz]	GW freq. derivative $\dot{f}$ [Hz/s]	RA [rad]	DEC [rad]	Epoch $\tau_{0\mathrm{SSB}}$ [MJD]	Proj. semi-major axis, a sin i [light-s]	Binary Period [s]	Eccentricity	Arg. of Periastron ω [rad]	Distance [pc]
J2204	≈ 23.6	-3.652×10^{-17}	5.7802112	0.4715040	56 805.0	210.680 632 593	70 437 206.112 106 89	0.00152	0.1118	2150
J1411	≈ 32.0	-4.904×10^{-17}	3.7145600	0.4512083	57 257.864 168	9.204 790 917	226 010.025 751 146 63	0.16993	1.4209	977
J0709	≈ 58.1	-6.418×10^{-16}	1.8724740	0.0869343	56 983.893 691	15.716 582 025	377 281.177 142 285 1	0.00023	5.6319	1790
J0824	≈ 202.8	-3.021×10^{-15}	2.2009213	0.0081476	56 600.0	18.988 928 488	2 005 081.527 370 442	0.00023	0.8084	1530
J0732	≈ 489.0	-7.344×10^{-16}	1.9749503	0.4057610	58 000.0	10.625 842 295	2 611 878.684 258 217 5	0.00001	1.1879	1660
J0509	≈ 493.1	-5.366×10^{-16}	1.3498838	0.1560374	57 384.0	2.458 025 534	424 049.203 613 615 9	0.00002	0.5642	1450
J0154	≈ 845.8	-1.046×10^{-15}	0.5001010	0.3240047	56 900.0	-	-	-	-	860